Electronic Supplementary Information

Directional imbalance of Bloch surface waves for ultrasensitive displacement metrology

Ruxue Wang[ab ‡], *Xinrui Lei*[cd ‡], *Yi Jin*[e], *Xiaolei Wen*[f], *Luping Du*[c*], *Aimin Wu*[ab,*], *Anatoly V. Zayats*[d], *Xiaocong Yuan*[c]

[‡]These authors contributed equally to this work.

[a]State Key Laboratory of Functional Materials for Informatics, Shanghai Institute of Microsystem and Information Technology, CAS, Shanghai, 200050, P.R. China

[b]Center of Materials Science and Optoelectronics Engineering, University of Chinese Academy of Sciences, Beijing, 100049, P.R. China

[c]Nanophotonics Research Center, Shenzhen Key Laboratory of Micro-Scale Optical Information Technology & Institute of Microscale Optoelectronics, Shenzhen University, Shenzhen, Guangdong, 518060, P.R. China

[d]Department of Physics and London Centre for Nanotechnology, King's College London, London, Strand, London, WC2R 2LS, United Kingdom

[e]Department of Optoelectronic Information Engineering, Zhejiang University, Hangzhou, Zhejiang, 310007, P.R. China

[f]Center of Micro- and Nanoscale Research and Fabrication, Hefei National Laboratory for Physical Sciences at Microscale, University of Science and Technology of China, Hefei, Anhui, 230026, P.R. China

*Correspondence and requests for materials should be addressed to L.D. (email: lpdu@szu.edu.cn) or to A.W. (email: wuaimin@mail.sim.ac.cn).

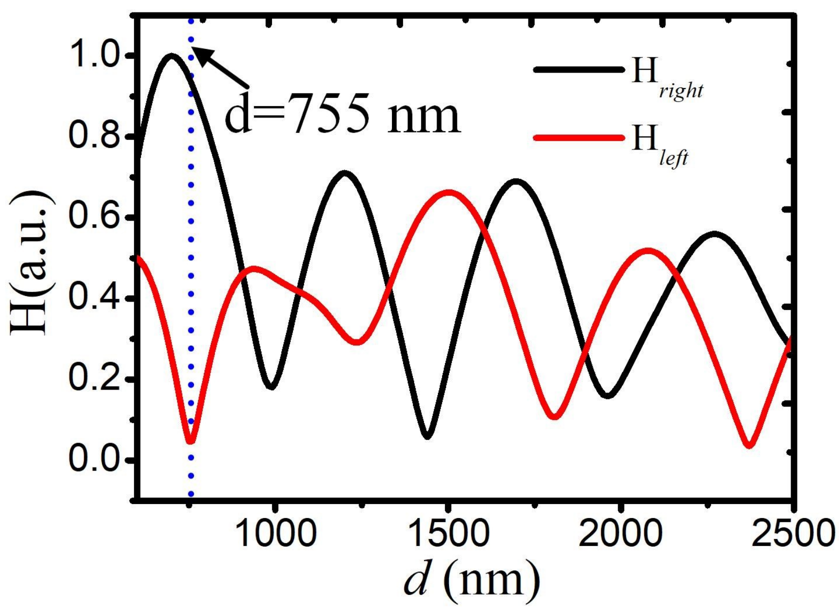

Fig. S1 Amplitude of the BSW magnetic field as a function of a distance between two nanoslits (centre-to-centre). Blue dotted line indicates an optimal distance of d=755 nm to achieve the maximum extinction ratio.

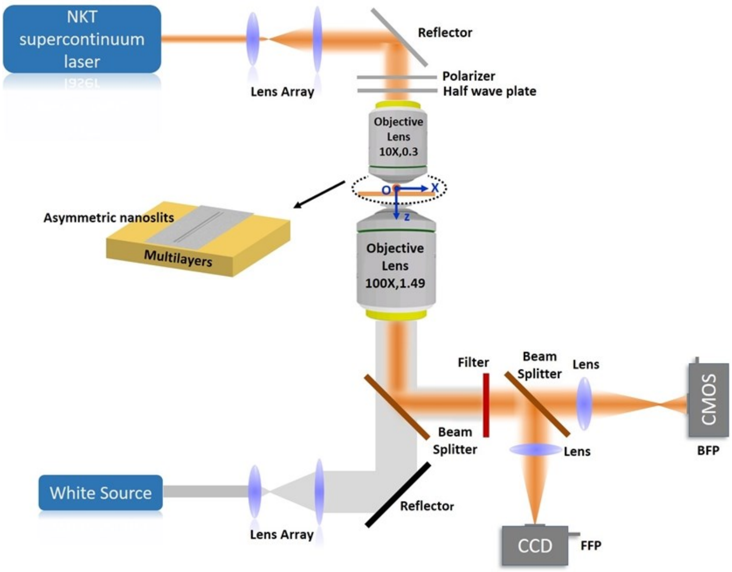

Fig. S2 Schematic diagram of the optical setup for leakage radiation microscopy (LRM). The back focal plane (Fourier plane image) and front focal plane (direct-space image) of the objective can be imaged onto two cameras (CCD and CMOS). Two sources are used to characterize the sample: a white light source tightly focused by the objective (x100, NA=1.49) is used to measure the reflected white BFP of the dielectric multilayer and a supercontinuum laser (range from 450 to 700 nm) focused by a low power objective (x10, NA=0.3) is used to excite the asymmetric BSW by an asymmetric double slit. The two sources are switched on or off as required but not turned on simultaneously. A polarizer and half-wave plate are used to control the polarization of the incident beam without changing the intensity.

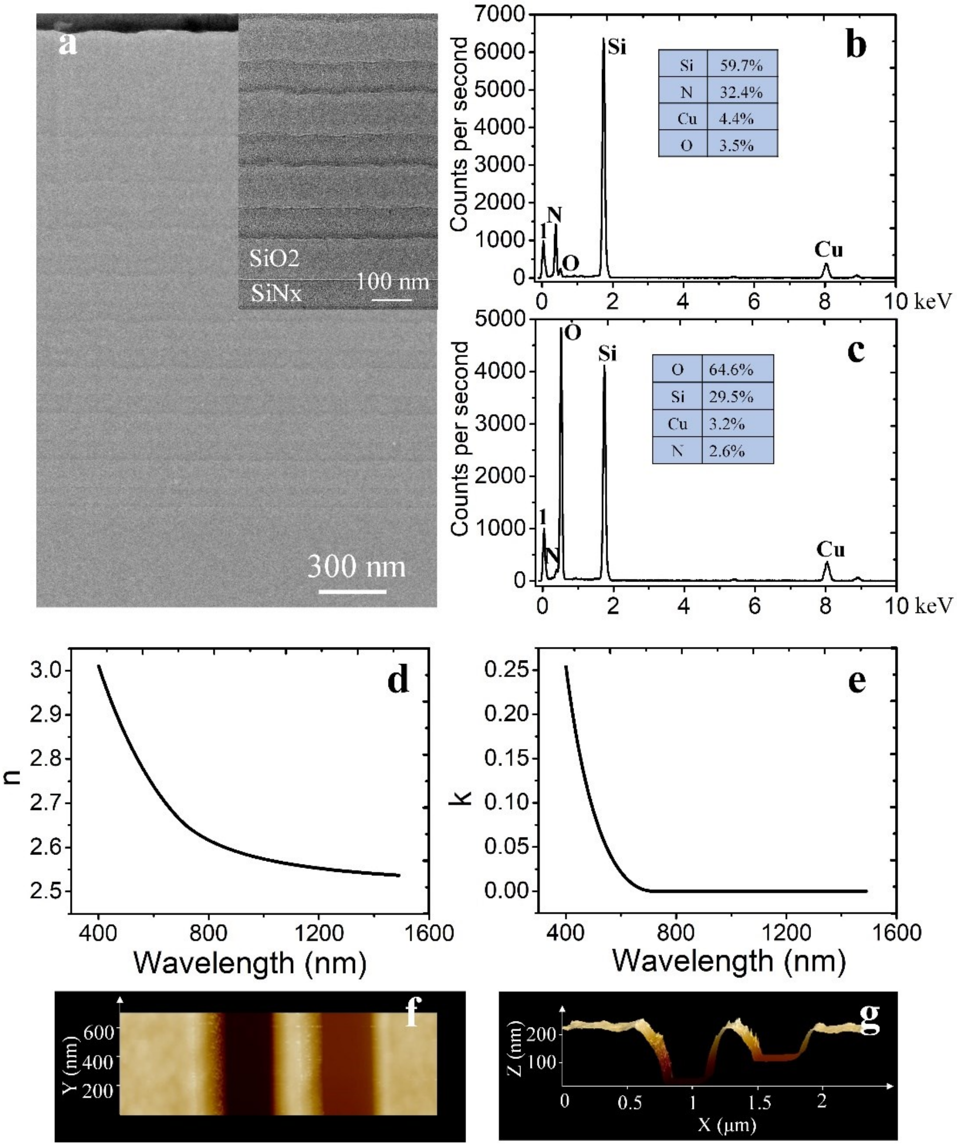

Fig. S3 Structural characterization. (a) Cross-sectional TEM (transmission electron microscope) image of the dielectric multilayer on a glass substrate. A scale bar is 300 nm. The inset is the zoomed region of the image. The thicknesses of a SiO_2 and SiN_x layers are about 100 nm and 80 nm, respectively. The scale bar is 100 nm. Energy dispersive spectrometer (EDS) spectra of SiN_x (b) and SiO_2 (c). The SiN_x is Si rich. Both spectra contain the Cu element used for the FIB cutting of the dielectric multilayer. Peak-1 is the calibration peak. (c) Real part of the refractive index of SiNx and (e) the imaginary part of the refractive index. (f-g) Atomic Force Microscopy (AFM) images of asymmetric slits. (f) is the 2D AFM image and (g) is the corresponding 3D morphology image.

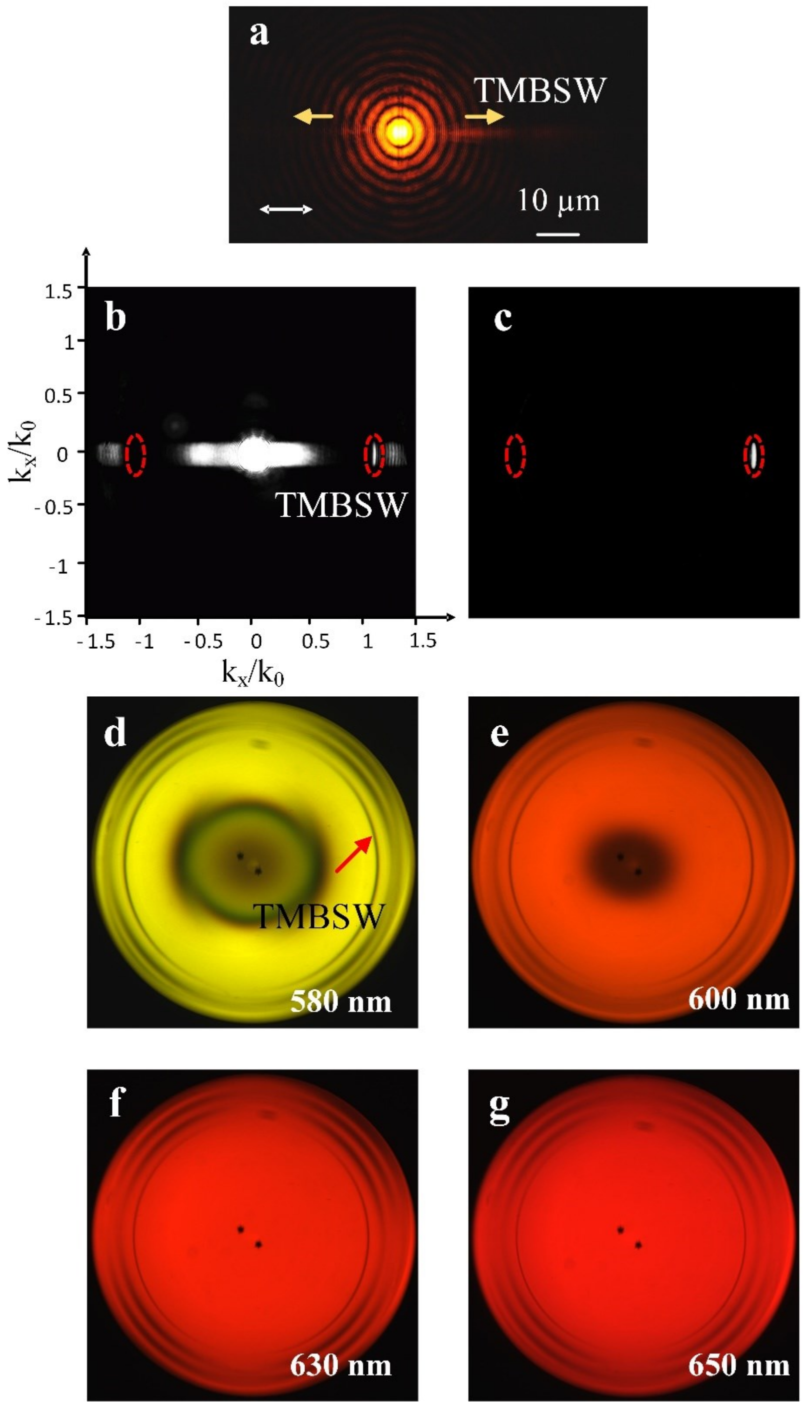

Fig. S4 Laser scattered and white light reflected BFP images from the dielectric multilayer. (a) Real space image at a wavelength of 600 nm corresponding to BFP images in *k*-space. The yellow single arrows represent the propagation direction of BSW. (b) BFP image as recorded. (c) Post-processed BFP image containing only the BSW signal with the incident Gaussian beam and other scattered light filtered out. The red dashed ovals indicate the BSW radiation. (d-g) Reflected white light BFP images. An expanded white light beam was used to fill the rear aperture of the oil-immersed objective (x 100, NA=1.49). The reflected beam in the BFP was then imaged onto a CCD camera. The dark dip represents the excitation of the BSW mode. From the known NA, the wavenumbers (or the effective indexes) of the BSW mode at different wavelengths (d–g) are derived to be approximately $1.16k_0$, $1.115k_0$, $1.063k_0$, and $1.022k_0$. The double-headed white arrow in (a) indicates the orientation of the incident light polarization. The orientation of the dark arcs on (d–g) confirms that the BSW at the dielectric multilayer can be excited by the TM polarized light.

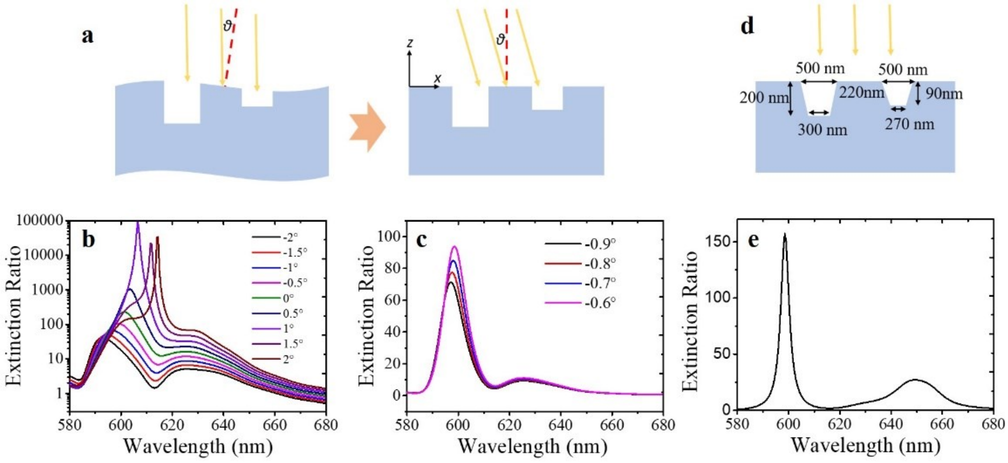

Fig. S5 Simulated extinction ratio spectra considering roughness of the multilayer and imperfect shape of nanoslits. (a) Schematics of the double slit in the multilayer with varying profile due to roughness which results in the incident angle deviation from the normal. (b) Wavelength dependences of the directional BSW excitation for different tilt angles from -2º to 2º. (c) Zoom in (b) for the angle range from -0.9 º to -0.6 º. (d) Cross-sectional profile of the fabricated nanoslits. (e) Wavelength dependence of the directional BSW excitation for trapezoidal shape of the slits.

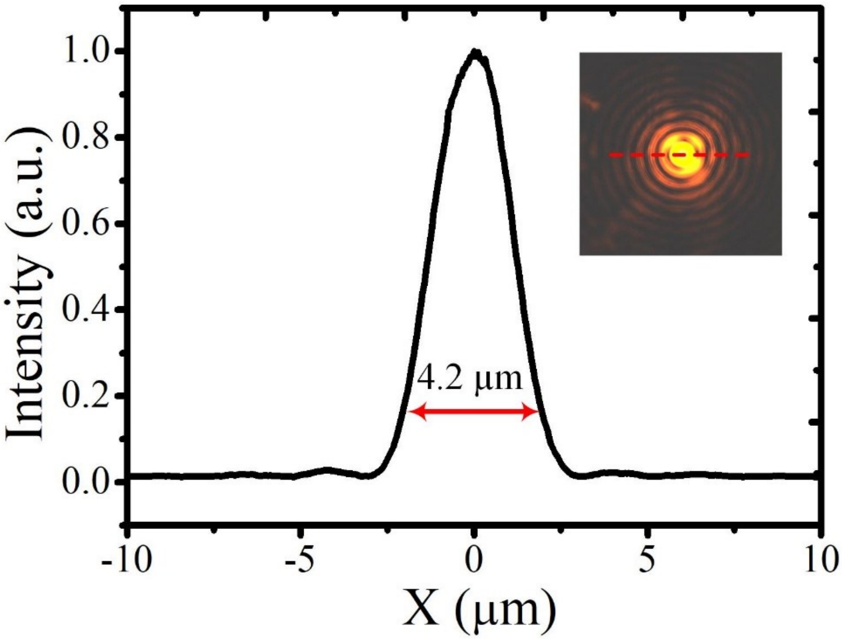

Fig. S6 Gaussian cross-section profile. A line profile of the incident Gaussian beam along the red dotted line in the inset. The waist radius is approximately 2.1 μm.

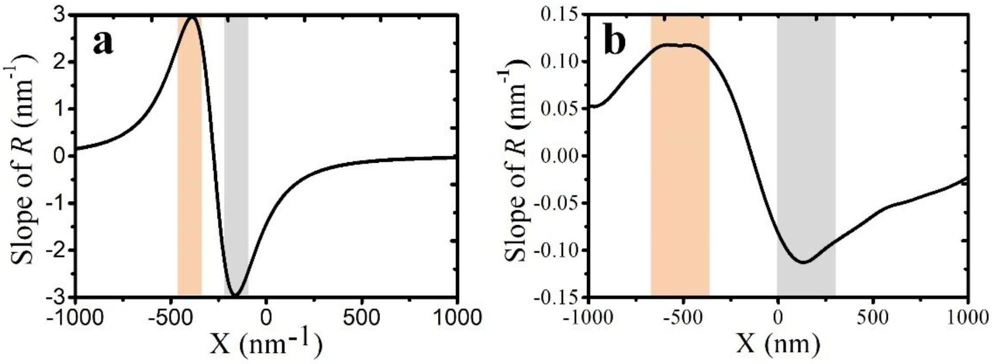

Fig. S7 Dependence of δR/δx from Eq. (2) on a lateral position. (a) Simulated and (b) experimental variations of *R* with the lateral position of the double slit with respect to a Gaussian beam (waist radius is about 2.1 μm). Compare to Figures. 4(a) and (d). The areas within the orange and gray shadings indicate the two ranges where the variation of *R* with the distance can be considered as linear. All other parameters are as in Fig. 4.

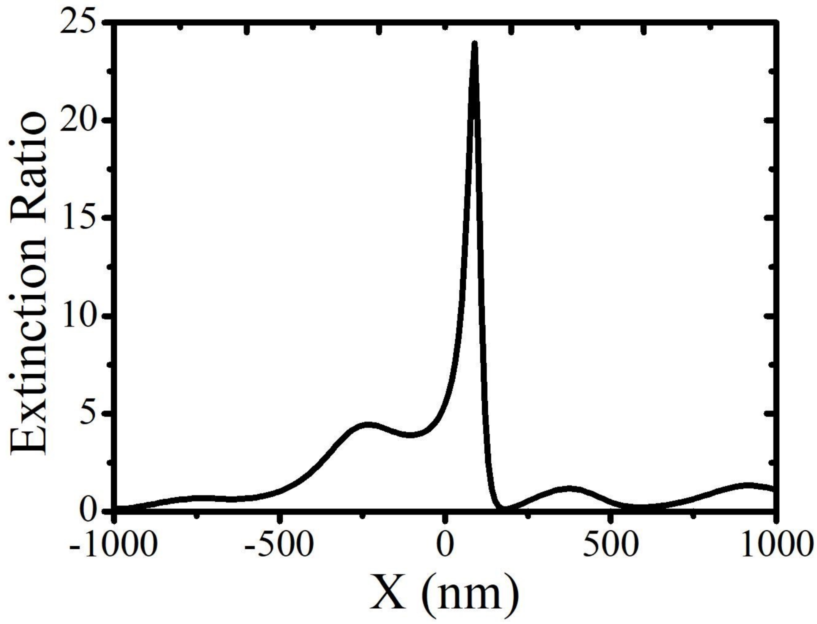

Fig. S8 Extinction ratio as a function of lateral position under the illumination with tightly focused (NA=0.9) Gaussian beam. Additional transverse phase leads to multiple peaks, high resolution, and small linearity range.

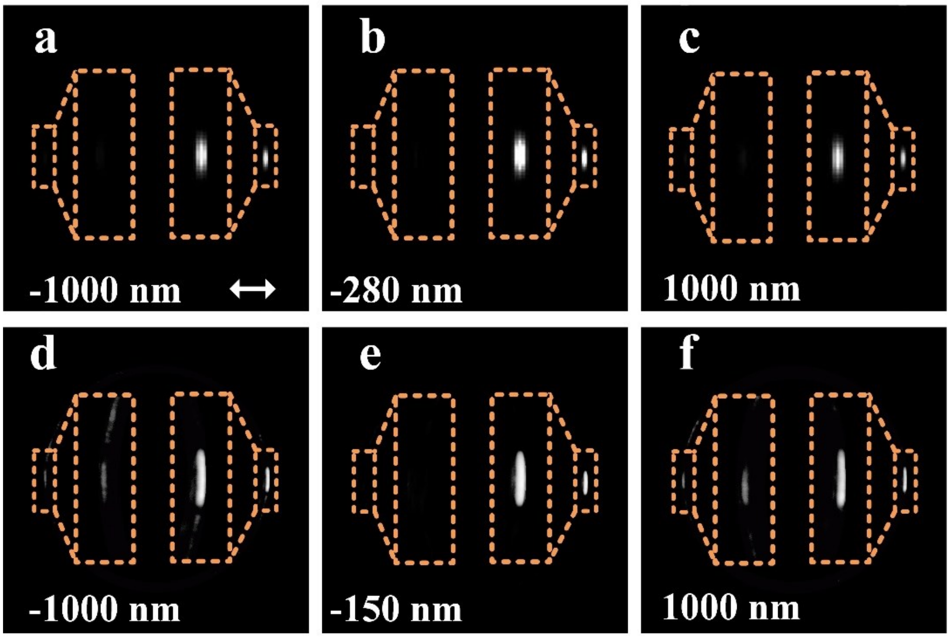

Fig. S9 BFP images for typical positions of the beam with respect to the double slit. (a-c) Simulated BFPs at the positions −1000 nm, −280 nm (peak of the R curve), and 1000 nm, respectively. The white double arrows indicate the direction of polarization. (d-f) The experimental images at the positions −1000 nm, −150 nm (peak of the R curve), and 1000 nm, respectively.

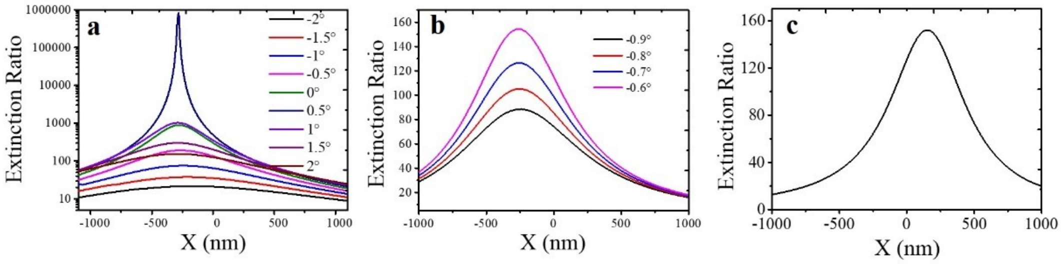

Fig. S10 Simulations of the displacement sensing with the directional BSWs considering roughness of the multilayer and a trapezoidal shape of the nanoslits. (a) Relation between R and the lateral displacement for different tilt angles from -2º to 2º. (b) Zoom in (a) for the angle range from -0.9 º to -0.6 º. The simulated sensitivity is comparable with the experimental results. (c) Simulation of the displacement sensing with the directional BSWs for a trapezoidal shape of the nanoslits in Fig. S5(b).

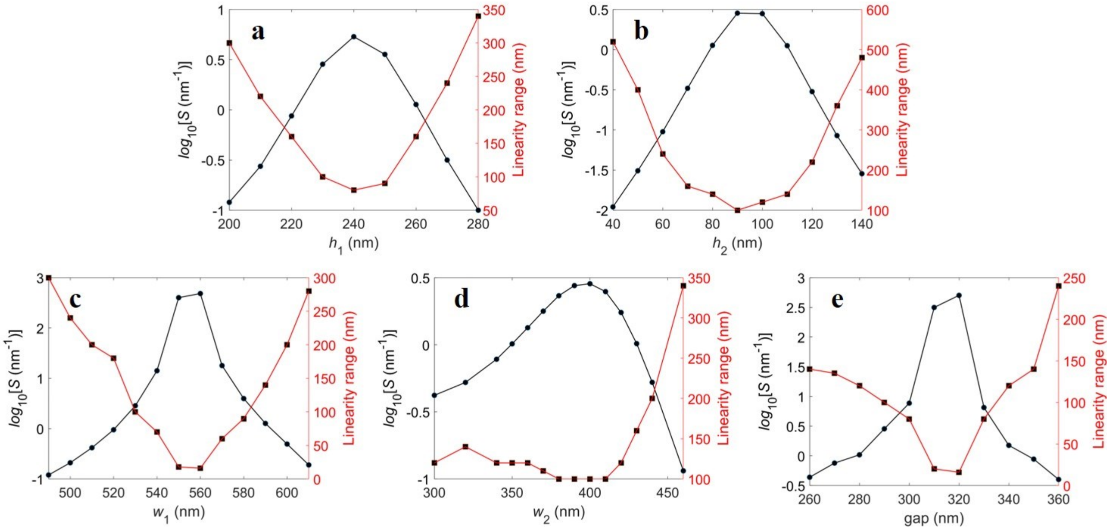

Fig. S11 Simulations of sensitivity and linearity range for different slit parameters considering fabrication tolerance. (a-b) Dependence of *S* and linearity range on slit depth. (c-d) Dependence of *S* and linearity range on slit width while keeping the same gap distance between the two slits. (e) Dependence of *S* and linearity range on gap distance.

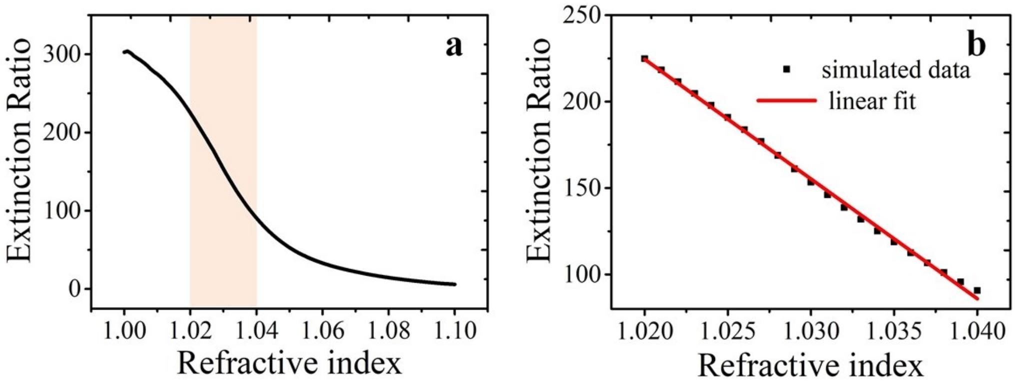

Fig. S12 Refractive index sensing based on directional imbalance of BSWs. (a) Simulated dependence of the extinction ratio on the refractive index of a superstrate under the illumination with a Gaussian beam (the waist radius is about 2.1 μm) for a fixed wavelength (600 nm) and fixed position. The sample parameters are as in Figure. 2. (b) Linearity range in the area within orange shading in (a). The error bars correspond to the residual obtained from the linear fitting.